2018 IEEE International Conference on Robotics and Automation (ICRA)
May 21-25, 2018, Brisbane, Australia

Ultra-Wideband Radar for Robust Inspection Drone in Underground Coal Mines

Fernando Cunha and Kamal Youcef-Toumi[1]

Abstract— **Coal mines pose a high safety risk for human workers. An autonomous inspection drone would enable a coal mine operation to reduce this risk by minimizing the time spent by workers inside the mine. This inspection drone must be highly robust to the harsh and dangerous environment of an underground coal mine, with high levels of coal dust and humidity that can obstruct many conventional sensing methods. For high functionality, the drone must sense and avoid potential obstacles and as well as inspect and map the mining wall face. The objective of this paper is to present ultra-wideband (UWB) radar as a robust sensing solution to this challenging environment and validate its performance experimentally in the typical coal mine environment, both statically and dynamically.**

I. INTRODUCTION

A. Coal Mine Risks

Coal mining poses many risks for human workers, several of which often prove fatal. Though coal mining is a relatively safe practice in the United States with 8 recorded deaths in 2016 [1], in 2010 there were over 2000 recorded coal mining deaths caused by accidents in China [2]. These deaths are caused primarily by ceiling collapse and gas related accidents [2].

A significant number of coal miners also perish each year due to chronic, as opposed to acute, heath issues. Over 6000 perish each year in China from pneumoconiosis, commonly referred to as "black lung disease." This disease is caused by the inhalation of dust into the lungs over long periods of time [3].

A primary reason for the large number of coal related deaths in China is the large amount of coal produced. From 1992 until 2010 China produced over 1 billion tons of coal each year, making up over 70% of China's energy use [2]. China has limited petroleum resources, and coal energy has been paramount to the economic development of China over the past 60 years [2]. For these reasons, coal use has only grown in China, and coal mine related accidents and deaths remain a serious issue in this industry.

B. Automation in Coal Mines

To reduce this loss of life, automation is being explored in the mining industry. The goal of this automation is to remove human workers from the mining wall face to mitigate the risk associated with coal mining. The autonomous, or semi-autonomous, mining equipment could then be supervised and operated from a safe base station, without any airborne coal dust, risk of mining accidents, or machinery operating nearby. This would ensure the safety of the of the human workers without affecting the production of the mine.

This study explores in particular an autonomous inspection drone. The purpose of this inspection drone would be to navigate a coal mine while streaming high definition video to a worker in a safe location, allowing this worker to observe the mining equipment and ensure normal operation from afar.

In order to navigate successfully, any autonomous equipment must be capable of detecting obstacles and avoiding them. Obstacle detection is a key factor in autonomous navigation, and will be the principal focus of this study. Any partially or completely autonomous vehicle must be able to sense its surroundings, determine if an obstacle bars its path, and select a new path that avoids this obstacle. This requires a reliable sensor to detect any potential obstacles, and in the particular case of a coal mine, this sensor must also be robust to the adverse conditions present.

This study analyzes different sensor options, selects an appropriate sensor for obstacle detection in a coal mine environment, and then validates experimentally that this sensor is robust to the expected conditions in a coal mine.

C. Sensing Challenges

The coal mine environment poses many challenges for obstacle detection and navigation. The primary challenge is the high concentration of coal dust that may obscure the view of the sensors. The partner company of this study has given 1 mg/m^3 as the typical airborne coal dust concentration in a coal mine, with a peak level at approximately 4 mg/m^3, though these levels may vary based on the type of mine and any measures taken to reduce dust levels. These were used as baseline values for the tests performed in this paper. Figure 1 illustrates the dusty conditions common in coal mines,

Fig. 1. A longwall shearer with water sprayers [4]

[1]Fernando Cunha and Dr. Kamal Youcef-Toumi are with the Mechatronics Research Laboratory, Department of Mechanical Engineering, Massachusetts Institute of Technology, Cambridge MA 02139 USA fcunha@mit.edu, youcef@mit.edu

as well as showing a longwall shearer, a device used to grind into the wall of a coal mine, with many water sprayers attached for dust mitigation [4].

Another potential challenge is the high humidity. To reduce the amount of airborne dust, water is constantly sprayed onto the wall face, resulting in high levels of moisture present in the air. The typical humidity level, also provided by the partner company, is approximately 95% relative humidity, reaching up to 100% in peak conditions. These values will again vary as different mines may employ varying techniques of dust mitigation.

The high humidity and dust concentrations present the most challenging adverse conditions when navigating through a coal mine environment. As a result, these were selected as the primary adverse conditions to be tested in this study.

II. SENSOR SELECTION

A. Common Sensing Methods

Several sensing technologies are commonly used in existing drones, both in industry and research. DJI, a leading commercial drone manufacturer, uses stereo vision, ultrasonic sensors, and dual redundant IMUs in their drones [5]. A new model of theirs, the Phantom 4 Pro, is also the first to include infrared sensing as well [5].

Various studies have explored ultrasonic sensors, commonly used as the most popular, low-cost sensor for obstacle detection [6], [7], [8], while infrared sensors, stereo cameras, and laser range finders (LRFs) are also typical sensors used frequently in obstacle detection studies [6], [7], [8], [9], [10].

Ultrasonic (US) sensors are simple and low cost, making them attractive for many applications. They detect obstacles by emitting high frequency sound waves, receiving reflected sound waves, and then using time-of-flight to determine the distance to the obstacle. They are the only common sensing method described that are not based on electromagnetic (EM) waves. US sensors struggle to detect sound absorbing materials like clothing, typically have low accuracy, and have shorter range than most other detection methods [6], [8].

Infrared (IR) sensors are fairly low-cost obstacle detection sensors that detect emitted infrared waves; all objects above absolute zero radiate some energy in the infrared spectrum, and the hotter the object the more energy is emitted. Infrared sensors detect these emissions and are commonly thought of as heat sensors. IR sensors are capable of detecting people well, but have limited resolution [6], [9]. IR sensors are more robust than some optical sensors in that they can easily see through fog or smoke, day or night, but they struggle to see through thick dust and are easily distorted by flames or other powerful heat sources [9].

Stereo cameras are commonly used as well, utilizing two or more lenses to create a 3D image, similar to how we process images from both our eyes to see in three dimensions. Stereo cameras are capable of high resolution and accuracy, provided the environment remains clear. Their performance will immediately drop in any smoke, fog, or dust, as optical wavelengths of light do not penetrate these conditions.

Laser range finders (LRFs) are more expensive but commonly used as well. LRFs emit a laser beam in the visible spectrum, receive a reflected wave, and then use time-of-flight to determine the distance to the target. This is the exact same principle as US sensors, but with optical wavelengths of light. However, as with stereo cameras, they are based on optical wavelengths and are unsuitable in conditions of smoke, fog, dust, or other adverse conditions.

B. Robust Sensing Selection

Ultrasonic sensors were the only sensors discussed that are robust to the conditions present in a coal mine [6], [8]. However, due to its low accuracy, relatively short range, and inability to detect clothing or soft materials, it was not selected for further testing. An inspection drone must be able to detect and avoid collisions with workers inside the mine. After testing an unmanned ground vehicle combining a ring of US sensors and LRFs, [8] found that though functional in smoky conditions, the US sensors were markedly less accurate and noisy when operating on their own.

In the literature review above, ultra-wideband (UWB) radar was also presented as an alternative to US [8]. UWB radar, an overlooked sensor method that has grown in popularity recently, provides similarly robust performance compared to US, but with stronger accuracy capabilities [8]. This technology was explored and ultimately selected as the best option for obstacle detection in an underground coal mine.

III. ULTRA-WIDEBAND (UWB) RADAR

UWB radar sensors have many features that make them strong candidates for use in underground coal mines. Primarily, like US, they are robust to conditions of smoke, fog, dust, rain, snow, gas, and aerosols, but are more accurate and have higher resolution and range [8], [11]. This is a key requirement for an underground coal mine. UWB power consumption is small, typically below 1 Watt [12], a necessity in this application to prevent the sensors from significantly reducing flight time. Further, due to the nature of UWB emissions, the power spectral density of the sensors are low, causing minimal interference with other wireless electronics such as the flight controller and telemetry link [12]. These sensors can identify various features such as edges, corners, and walls, as well as provide three dimensional coordinates for the nearest detected object [13]. Finally, as UWB encompasses a large bandwidth of radio waves, it is more robust to a variety of targets; target radio wave reflection is often frequency dependent, so having multiple frequencies present increases robustness to this error [12].

In industry as well, radar has been growing in popularity particularly with automotive manufacturers [11]. Audi, BMW, Cadillac, Lexus, and Mercedes vehicles now have adaptive cruise control or active brake assist features that utilize radar sensors [11].

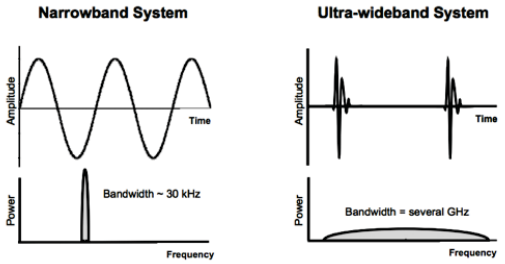

Fig. 2. Comparison of wideband and narrowband radar systems [15]

Fig. 3. The Walabot Pro UWB Radar sensor [16]

A. Radar Principles

Like US and LRF sensors, radar utilizes time-of-flight to characterize the distance to a measured target. Radar utilizes electromagnetic waves in the radio spectrum. These radio waves have much longer wavelengths than visible or infrared light, giving them different propagating characteristics. In this case, this is beneficial, as radio waves are much more capable of penetrating dust and smoke than visible light waves [14].

UWB radar is a subset of radar systems that have relatively large bandwidths [11]. Conventional narrowband systems transmit continuous waveforms at a specific frequency, resulting in a small bandwidth and high power spectral density. UWB systems transmit brief, impulse-like waveforms, resulting in a large bandwidth and a low power spectral density spread out across a large range of frequencies. Figure 2 illustrates a simple, conceptual comparison between narrowband and wideband systems. The pulse width in UWB systems is usually between 100 picoseconds and a few nanoseconds, which corresponds to a frequency range of several GHz [15].

The larger bandwidth results in different characteristics and applications for UWB systems. Primarily, having a lower peak power reduces the achievable range of the sensor. If the returning signal power density is too low, it cannot be reliably detected. UWB radar systems are commonly used in short range applications, on the order of meters, in comparison to narrowband systems which can achieve ranges on the order of kilometers [14], [15]. However, UWB systems consume much less power. This makes UWB radar more feasible for portable, low-power systems. In simple terms, UWB can be thought of as a low-power, short range radar system. This makes it ideal for use as a sensor on a drone; UWB radar can provide the accuracy, resolution, and detail of a typical radar system with low power consumption and a shorter range.

IV. STATIC TARGET DETECTION

A. UWB Radar Sensor Selection

The Walabot Pro UWB Radar sensor, shown in Figure 3, was selected as the UWB sensor for use in this study. The Walabot sensor is relatively low-cost at $600 but is still fully programmable and developer friendly, with an SDK kit that is compatible with Windows, Linux, Android, and Raspbian. The United States model of the sensor operates at the Federal Communications Commission approved frequencies of 3.3-10.3 GHz, and connects to a computer via microUSB.

The sensor was initially run through simple characterization tests, in ideal conditions, with a clear view and a large metallic plate as the chosen target. The Walabot consistently achieved accuracies on the order of cms up to a range of 4 m and a resolution of approximately 0.5 cm, all with a repeatability on the order of microns. In good conditions, the Walabot has very strong accuracy, resolution, and repeatability.

B. Experimental Design

To create a contained test environment with controlled conditions, a test setup was assembled inside an acrylic box measuring 40 x 40 x 40cm. Five brushless fans, two Honeywell humidity sensors, and two Sharp optical dust sensors were placed inside the box to measure the conditions inside the test environment. Weathering tape was then placed down around the top edges of the box to seal the lid and prevent dust or moisture from escaping during testing.

To mount the Walabot sensor in a fixed location on the outside of the box, four L shaped brackets were attached to the box in such a way to provide a slip fit for the sensor, labeled D in Figure 4. The sensor could then simply be gently pressed into the slot, and gently pulled out after testing. The sensor was mounted outside the box to ensure the dust or moisture wouldn't damage it. As radar is capable of penetrating through acrylic, this will protect the sensor without preventing it from detecting the target inside. For a

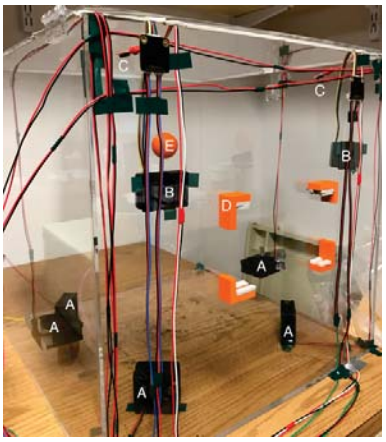

Fig. 4. Adverse environment testing setup. A are fans, B are dust sensors, C are humidity sensors, D is radar mount, E is static / dynamic target.

fixed target location, a small peg was attached to the inside of the box. For all tests discussed in this section and the next, a spherical target was used, labeled as E in Figure 4. For reference, all future mentions of the 'sensor' refer to the UWB radar sensor, unless explicitly stated otherwise.

C. Harsh Environment Testing

The primary goal of this testing is to illustrate, quantitatively, that the UWB radar sensor readings are unaffected by the addition of coal dust or moisture into the environment. To achieve this primary goal, the change in sensor readings when coal dust or moisture is added to the environment is compared to a test termed the control test. If the change from sensor readings during adverse tests is the same as the change in the control test, this indicates that adding the adverse environmental conditions does not affect sensor performance. The control test will capture any changes caused by sensor noise, multipath errors in the box, vibrations from the fans, and any other errors that may affect sensor readings.

To determine the moisture level inside the test environment, the humidity sensor readings were used to determine a relative humidity value in percentage, %RH. Determining the airborne coal dust concentration was slightly more complex as the desired concentration level, 4 mg/m^3, exceeds the maximum dust sensor limit of 0.5 mg/m^3. To accurately obtain data at higher dust concentrations, data from the dust sensor at low concentrations was correlated to video data shot on an iPhone 7. This video data was analyzed frame by frame in MATLAB to develop a linear correlation matching a change in pixel intensity to a particular dust concentration up to the saturation level of the dust sensor. Figure 5 shows frames from one of these videos. This correlation was then used to determine the airborne dust concentration at high dust levels using only video data.

The radar sensor was then tested at four different coal dust concentration levels. The total amount of coal dust placed in the box, the average change in pixel data calculated from the iPhone videos at each dust level, and the corresponding calculated airborne coal dust concentrations are shown in Table I, below. Uncertainty values represent a 95% confidence interval.

Fig. 5. Frames from iPhone video data before and after fans were turned on, with 24g of coal dust inside environment

TABLE I
CALCULATED DUST CONCENTRATION LEVELS BEYOND DUST SENSOR SATURATION

Total Amount of Dust in Test Environment	Average Increase in Pixel Intensity	Airborne Dust Concentration [mg/m^3]
8g	16.11 $\pm$ 0.30	1.85 $\pm$ 0.23
16g	25.72 $\pm$ 0.10	2.96 $\pm$ 0.31
24g	31.13 $\pm$ 0.15	3.59 $\pm$ 0.38
32g	37.07 $\pm$ 0.31	4.27 $\pm$ 0.47

In all test scenarios, five different trials were performed. In the control test, the radar sensor was placed into the mounting bracket and initialized to an empty test environment. Then, the orange, spherical target labeled E in Figure 4 was placed on the peg inside the test environment. Data was recorded for 30 seconds, termed the 'start' data, and then the fans were turned on. Data was then recorded again for another 30 seconds, termed the 'end' data. This was repeated five times, for all test scenarios.

Then the same process was repeated with the addition of moisture or dust into the test environment. With moisture, water was sprayed into the test environment with the target. After the fans were turned on, the humidity level in the box rapidly increased to approximately 100% RH, taking approximately five minutes to stabilize at a saturated relative humidity. The same initial 30 seconds of start data was recorded, and then 30 seconds of end data was recorded after both humidity sensors read 99% RH or above.

For the coal dust testing, for each of the four levels, the coal dust was measured and added in prior to any testing. Then the exact same process as the control was followed, but when the fans are turned on, they kick up the dust to create the desired dusty environment. Again, the same start data set was recorded initially, and after one minute to allow the dust concentration to reach a steady state, the end data set was recorded.

Each data set includes a timestamp, x value, y value, and z value for the center of the detected target. To analyze this data, for each axis the change between the averages of the start and end data sets was calculated, along with a 95% confidence interval for that difference. 50 points from each data set were used when calculating averages and confidence intervals. Then, for each test scenario, the five differences from each of the five trials were averaged together, and again a 95% confidence interval was calculated.

If the harsh environment is affecting radar sensor performance, this should be reflected in a larger change from start to end in the humidity or dust tests, relative to the control. If the changes from start to end are similar in all tests, this implies that the harsh environment is not affecting sensor performance. If there is no discrepancy, any non-zero change from start to end must be caused by factors unrelated

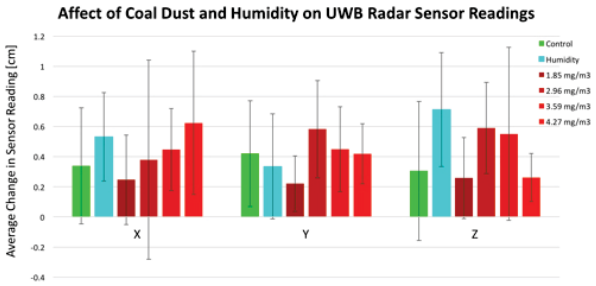

Fig. 6. Static target UWB radar testing in adverse conditions. Error bars show 95% confidence intervals.

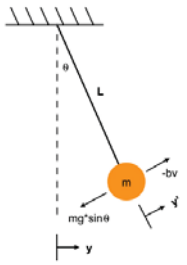

Fig. 8. Target pendulum motion free body diagram

to the harsh environment, such as vibration from the fans, multipath errors, inherent noise in the sensor, or the acrylic layer interfering with sensor performance.

Figure 6 illustrates all the collected data for testing performed with a static target. The columns are split into each axis, as the data from each axis was analyzed separately. The green column to the left represents the control, the light blue represents humidity data, and all the red columns represent coal dust data at the four levels described previously. The coal dust concentration increases from left to right, with the rightmost, brightest red column representing the highest coal dust concentration at 4.27 mg/m3. The y axis in the figure represents the average delta value calculated between start and end data sets for the respective test scenario.

This figure illustrates that the average changes for all five adverse tests fall within the error bars of the control data, indicating there is no significant difference in the radar sensor performance caused by the adverse environmental conditions. The 95% confidence intervals of all test cases overlap with the control test. This implies that the radio waves in the frequency spectrum of the Walabot UWB radar sensor, 3.3 - 10.3 GHz, were successfully able to transmit through the tested levels of airborne moisture and coal dust, within the confidence intervals this experiment was able to achieve.

V. DYNAMIC TARGET DETECTION

A. Experimental Design

The Walabot sensor was then tested with a dynamic target. The success of the static test data may be because the average value over 50 data points was enough to reject any outliers caused by dust or moisture scattering. In a dynamic scenario, each data point will be analyzed individually. Should the data collected from the sensor remain accurate and repeatable in adverse conditions, as before, this will strengthen the claim that UWB radar is a robust solution for obstacle detection in harsh, real-world environments and scenarios.

The same test environment was used as with the static testing, except that the same spherical target was now placed on a pendulum, as shown in Figure 7.

A diagram of the pendulum free-body diagram, as seen by the sensor, is shown in Figure 8. As the static target tests demonstrate no significant change in performance along each axis, only data from the y axis is analyzed in this section. By balancing the forces in the y' axis of Figure 8, we can derive a differential equation for the motion of the target, as a function of θ,

$$\frac{d^2\theta}{dt^2} + \frac{b}{m}\frac{d\theta}{dt} + \frac{g}{L}\sin\theta = 0 \tag{1}$$

This governing equation was then solved numerically in MATLAB for the measured length, mass, and damping coefficient of the system, resulting in predicted y values for the pendulum system. This model was used as a baseline for all tests, shown in gray as the predicted data in later figures.

B. Harsh Environment Testing

For all tests in this section, the Walabot was programmed with the same arena as before, but with a moving target identification (MTI) filter applied. This is a temporal high filter that attenuates stationary objects.

Three different tests were performed with five trials taken for each test; a control test, a humidity test, and a coal dust test. For the test termed the control, there is no dust or excess moisture in the test environment. The fans are turned on and the pendulum is released, and data is recorded for 30 seconds. In the coal dust test, the only change is that 32g of coal dust is added into the box prior to testing. This is the peak

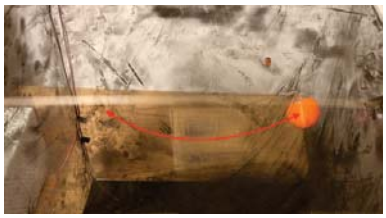

Fig. 7. Orange spherical target acting as a pendulum

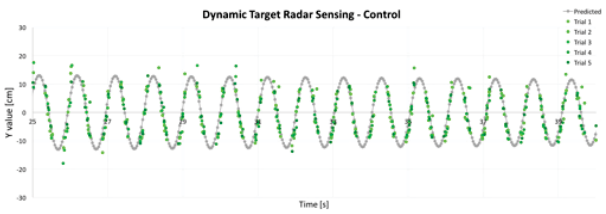

Fig. 9. Dynamic target control test of radar sensor, low velocity points removed

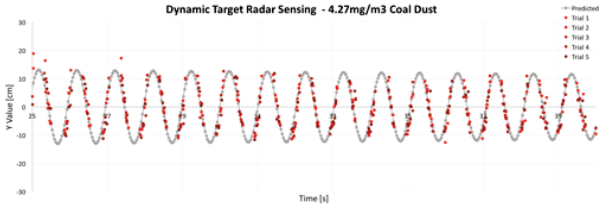

Fig. 10. Dynamic target coal test of radar sensor, low velocity points removed

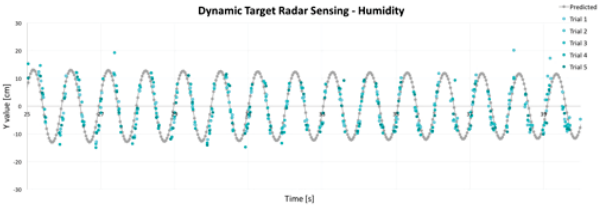

Fig. 11. Dynamic target humidity test of radar sensor, low velocity points removed

airborne coal dust level tested previously, at approximately 4.27 mg/m^3. For the humidity test, water is sprayed into the test environment and fans are turned on. Once the %RH surpassed 99%, the pendulum was released and recording began.

The MTI filter resulted in some large outliers at the peaks and valleys of the pendulum swing. As the target approached zero velocity before switching directions, it was filtered out. To remove this error, low velocity data points near these peaks were removed from the figures shown.

As Figures 9-11 illustrate, the coal dust and humidity tests are indistinguishable from the control tests. In all trials of all three scenarios, the sensor data closely matches the predicted pendulum model. This dynamic target data illustrates that each individual data point has a high level of accuracy, as each data point stays close to the predicted curve, with the exception of a few outliers that can be attributed to sensor noise. There is no noticeable discrepancy from trial to trial as well, indicating a strong repeatability is maintained despite adverse conditions.

This data, as does the data in the previous section, continues to support that UWB radar is a strong candidate for use on a drone in adverse environments, particularly in the conditions of a coal mine.

VI. ANOMALOUS PROPAGATION TESTING

A. Principles of Anomalous Propagation

Anomalous propagation (AP) is the term used to describe the phenomenon when atmospheric conditions cause radio waves to propagate in unexpected ways. In conventional radar systems, this is typically caused by temperature inversions or strong moisture gradients in the atmosphere [17]. This is because variations in temperature or moisture will affect the resulting refractive index of air [17]. This change in the refractive index of air will alter the path of the radio waves, resulting in skewed readings from the radar.

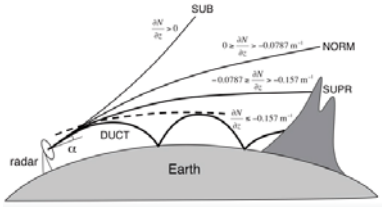

Fig. 12. Propagation regimes of a ground-based radar beam [18]

Figure 12 demonstrates the different types of AP commonly observed with long range radar systems. In the figure, α represents the small tilt angle of the emitted radar beam relative to the horizontal plane of the Earth's surface. The differing propagation regimes shown are subrefraction (SUB), normal refraction (NORM), superrefraction (SUPR), and ducting (DUCT).

The propagation regimes are labeled based on the refractivity gradient with respect to height, $\frac{\partial N}{\partial z}$. N is the refractivity of the air, and z is the height relative to the Earth's surface. This number indicates the rate at which the refractivity of air is varying as height increases. Refractivity N can be calculated from the refractive index n with equation (2),

$$N = (n - 1) \times 10^6 \tag{2}$$

For this study, our radar sensor must be able to maintain strong performance when mounted onto a drone, without anomalous propagation affecting the sensor readings. Similar to the atmospheric changes discussed above, the propeller air flow will result in varying air pressures and air densities, which will affect the index of refraction of the air near the propellers. Though it is expected this effect will be negligible due to the short range of UWB radar relative to conventional radar systems, it must still be verified experimentally as refractive index is an empirically determined value.

B. Experimental Setup

To illustrate that anomalous propagation will not occur when mounting UWB radar on a drone, the Walabot was mounted onto a static drone and tested with and without the propellers active. If propeller airflow skews the sensor readings, this will indicate anomalous propagation is occurring. If not, the sensor readings will remain consistent whether or not the propellers are on, indicating this effect is negligible.

Fig. 13. Anomalous propagation drone testing setup

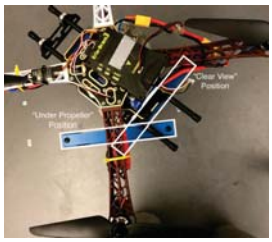

Fig. 14. Overhead image illustrating radar sensor mounting locations

The Erle-Copter drone was selected for testing. Figure 13 shows the test setup used in this section. To ensure the drone remained stationary it was bolted down onto a heavy mount. This mount also props the drone up to reduce the interference of ground effects on propeller airflow. The target stand and target used in this testing are also pictured.

The Walabot sensor was mounted underneath the drone. Two different mounting positions were used, as Figure 14 illustrates. The "clear view" mounting position gives the sensor an uninterrupted view of the target, while the "under propeller" position forces the sensor to look through the propeller airflow column.

C. Anomalous Propagation Testing

A similar test method to prior sections was used. First, the radar sensor was initialized to the empty table with the target stand. Then the target was placed on the stand and "start" data was recorded for 30 seconds. The drone was then powered on, and the throttle was placed at half power. Then 30 more seconds of "end" data were recorded with the propellers on. Five trials were performed for each of the two mounting positions. The "clear view" test is essentially the control test of this section, capturing any potential effects caused by drone vibrations, sensor noise, and multipath errors.

Figure 15 illustrates that there is no discernable change between the data sets. Along all three axes, the error bars from both mounting positions overlap. The average changes in sensor readings are on the order of 1mm, and no error bar exceeds 2.5mm, which is less than 0.2% the distance to the target. This is the largest possible discrepancy caused by anomalous propagation within the 95% confidence intervals. This small error is well within acceptable levels for the purposes of obstacle detection and avoidance. The collected data here clearly supports that mounting the radar sensor on the drone will have no noticeable effect on sensor performance, as both mounting points resulted in similar data.

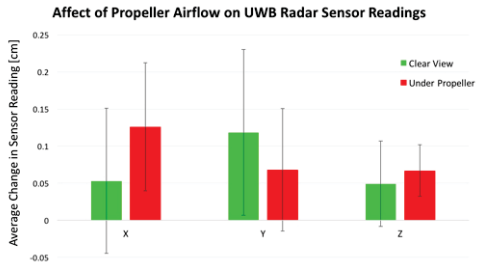

Fig. 15. Static target radar sensor testing in anomalous propagation conditions. Error bars show 95% confidence intervals.

VII. CONCLUSION

UWB radar technology is presented and analyzed for use on an inspection drone in underground coal mines. This technology was tested both in clear conditions and the adverse conditions expected in a coal mine, with up to 99% relative humidity and 4 mg/m3 of coal dust present. In both environments, the sensor maintained strong accuracy and repeatability. Further, no anomalous propagation effects were observed when tested with propeller airflow. UWB radar is a strong candidate for obstacle avoidance and navigation in robust environments like coal mines.

VIII. ACKNOWLEDGEMENTS

The authors thank the MIT Presidential Fellowship program and the Beijing Tiandi-Marco Electro-Hydraulic Control System Company Ltd for their support.

REFERENCES

[1] United States Department of Labor. Coal fatalities for 1900 through 2016. Online, 2017.
[2] X. He and L. Song. Status and future tasks of coal mining safety in China. Saf. Sci., 50(4):894-898, April 2012.
[3] H. Chen, Q. Feng, R. Long, and H. Qi. Focusing on coal miners' occupational disease issues: A comparative analysis between China and the United States. Saf. Sci., 51(1):217-222, January 2013.
[4] Center for Disease Control. History of the mining program. Online, Sep 2012.
[5] http://www.dji.com/. Dji official website. Online, 2017.
[6] N. Gageik, P. Benz, and S. Montenegro. Obstacle detection and collision avoidance for a UAV with complementary low-cost sensors. IEEE Access, 3:599- 609, 2015.
[7] J. F. Roberts, T. S. Stirling, J. C. Zufferey, and D. Floreano. Quadrotor using minimal sensing for autonomous indoor flight. Proc. MAV, pages 1-8, 2007.
[8] J. M. Santos, M. S. Couceiro, D. Portugal, and R. P. Rocha. A sensor fusion layer to cope with reduced visibility in slam. J. Intell. Robot. Syst., 80(3-4):401-422, December 2015.
[9] C. Brunner, T. Peynot, T. Vidal-Calleja, and J. Underwood. Selective combination of visual and thermal imaging for resilient localization in adverse conditions: Day and night, smoke and fire. J. Field Robot., 30(4):641-666, Jul-Aug 2013.
[10] Abraham Bachrach, Samuel Prentice, Ruijie He, and Nicholas Roy. RANGERobust autonomous navigation in GPS-denied environments. J. Field Robot., 28(5):644-666, Sep-Oct 2011.
[11] B. Yamauchi. All-weather perception for man-portable robots using ultrawideband radar. IEEE International Conference on Robotics and Automation, July 2010.
[12] R.J. Fontana, E.A. Richley, A.J. Marzullo, L.C. Beard, R.W.T. Mulloy, and E.J. Knight. An ultra-wideband radar for micro air vehicle applications. IEEE Conf. on Ultra Wideband Systems and Technologies, May 2002.
[13] J. Seitz, M. Schaub, O. Hirsch, R. Zetik, T. Deissler, R. Thoma, and J. Thielecke. UWB feature localization for imaging. IEEE International Conference on Ultra- Wideband, 2, 2008.
[14] J. C. Toomay and P. J. Hannen. Radar principles for the non-specialist. SciTech Pub., Edison, NJ, 3rd ed edition, 2004.
[15] C. N. Paulson, J. T. Chang, C. E. Romero, J.Watson, F. J. Pearce, and N. Levin. Ultra-wideband radar methods and techniques of medical sensing and imaging. SPIE International Symp. on Optics, Oct 2005.
[16] https://walabot.com/. Walabot official website. Online, 2017.
[17] A. V. Magaldi, M. Mateu, J. Bech, and J. Lorente. A long term (1999-2008) study of radar anomalous propagation conditions in the western mediterranean. Atmos. Res., 169:73-85, March 2016.
[18] P. Lopez. A 5-yr 40-km-resolution global climatology of superrefraction for ground-based weather radars. J. Appl. Meteorol. Climatol., 48(1):89-110, Jan 2009.